J|A|C|S
ARTICLES
Published on Web 08/13/2002

Structure and Properties of the Dendron-Encapsulated Polyoxometalate $(C_{52}H_{60}NO_{12})_{12}[(Mn(H_2O))_3(SbW_9O_{33})_2]$, a First Generation Dendrizyme

Dirk Volkmer,*,† Björn Bredenkötter,† Jörg Tellenbröker,† Paul Kögerler,‡ Dirk G. Kurth,*,§ Pit Lehmann,§ Heimo Schnablegger,⊥ Dietmar Schwahn,|| Markus Piepenbrink,# and Bernt Krebs*,#

Contribution from the Department of Inorganic Chemistry 1, University of Bielefeld, P.O. Box 100 131, D-33501 Bielefeld, Germany, Ames Laboratory and Department of Physics and Astronomy, Iowa State University, Ames, Iowa 50011-3160, Max Planck Institute of Colloids and Interfaces, D-14424 Potsdam, Germany, Institute for Physical Chemistry, University of Hamburg, D-20146 Hamburg, Germany, Institut für Festkörperforschung (IFF), Forschungszentrum Jülich GmbH, D-52425 Jülich, Germany, and Institute of Inorganic Chemistry, University of Münster, D-48149 Münster, Germany

Received November 26, 2001. Revised Manuscript Received May 21, 2002

Abstract: Combining analytical and theoretical methods, we present a detailed study of a heteropolytungstate cluster encapsulated in a shell of dendritically branching surfactants, namely $(C_{52}H_{60}NO_{12})_{12}[(Mn(H_2O))_3(SbW_9O_{33})_2]$, **3**. This novel surfactant-encapsulated cluster (SEC) self-assembles spontaneously from polyoxometalate-containing solutions treated with a stoichiometric amount of dendrons. Compound **3** exhibits a discrete supramolecular architecture in which a single polyoxometalate anion resides in a compact shell of dendrons. Our approach attempts to combine the catalytic activity of polyoxometalates with the steric properties of tailored dendritic surfactants into size-selective catalytic systems. The structural characterization of the SEC is based on analytical ultracentrifugation (AUC) and small-angle neutron scattering (SANS). The packing arrangement of dendrons at the cluster surface is gleaned from molecular dynamics (MD) simulations, which suggests a highly porous shell structure due to the dynamic formation of internal clefts and cavities. From analysis of the MD trajectory of **3**, a theoretical neutron-scattering function is derived that is in good agreement with experimental SANS data. Force field parameters used in MD simulations are partially derived from a quantum mechanical geometry optimization of $[(Zn(H_2O))_3(SbW_9O_{33})_2]^{12-}$, **2b**, at the density functional theory (DFT) level. DFT calculations are corroborated by X-ray structure analysis of $Na_6K_6[(Zn(H_2O))_3(SbW_9O_{33})_2]\cdot 23H_2O$, which is isostructural with the catalytically active Mn derivative **2a**. The combined use of theoretical and analytical methods aims at rapidly prototyping smart catalysts ("dendrizymes"), which are structurally related to naturally occurring metalloproteins.

Introduction

Polyoxometalates (POMs) constitute a structurally diverse class of discrete, negatively charged early transition metal oxide clusters.[1] Those POMs containing transition metal ions in their highest possible oxidation states have found widespread use as oxidation catalysts. According to Neumann and Hill[2] several major reaction modes of POM-catalyzed oxidation processes may be distinguished, depending on the chemical nature of the oxidant, which often is composed of molecular oxygen, peroxygen compounds (e.g. H_2O_2, or *tert*-butylhydroperoxide), or reactive transition metal-oxo species. In the latter case, "sandwich"-type transition metal substituted POMs have recently attracted much attention, owing to their enhanced solvolytic stability, their high turnover numbers in catalytic processes, and their ability to catalyze alkane oxidation[3] as well as alkene epoxidation[4] with high stereo- or regioselectivity.

Although many mechanistic details have yet to be elucidated, a conceptual drawback of homogeneous catalytic processes involving POMs is the lack of methods to direct the substrate toward the catalytically active center. In contrast to many

* To whom correspondence should be addressed. D.V.: Phone, +49 (0)521 106 6142; fax, +49 (0)521 106 6003; e-mail, dirk.volkmer@uni-bielefeld.de. D.G.K.: Phone, +49 (0)331 567 9211; fax, +49 (0)331 567 9202; e-mail, kurth@mpikg-golm.mpg.de. B.K.: Phone, +49 (0)251 83 33131; fax, +49 (0)251 83 38366; e-mail, krebs@uni-muenster.de.
† University of Bielefeld.
‡ Iowa State University.
§ Max Planck Institute of Colloids and Interfaces.
⊥ University of Hamburg.
|| Institut für Festkörperforschung.
University of Münster.

(1) (a) Pope, M. T.; Müller, A. *Angew. Chem., Int. Ed. Engl.* **1991**, *30*, 34. (b) Pope, M. T., Müller, A., Eds.*; Polyoxometalates: From platonic solids to antiretroviral activity*; Kluwer: Dordrecht, 1994.
(2) (a) Hill, C. L.; Prosser-McCarther, C. M. *Coord. Chem. Rev.* **1995**, *143*, 407. (b) Neumann, R. *Progr. Inorg. Chem.* **1998**, *47*, 317.
(3) (a) Neumann, R.; Khenkin, A. M. *Inorg. Chem.* **1995**, *34*, 5759. (b) Neumann, R.; Dahan, M. *Nature (London)* **1997**, *388*, 353.
(4) (a) Khenkin, A. M.; Hill, C. L. *Mendeleev Commun.* **1993**, 140. (b) Neumann, R.; Gara, M. *J. Am. Chem. Soc.* **1994**, *116*, 5509. (c) Neumann, R.; Gara, M. *J. Am. Chem. Soc.* **1995**, *117*, 5066. (d) Zhang, X.; Sasaki, K.; Hill, C. L. *J. Am. Chem. Soc.* **1996**, *118*, 4809.

catalytic systems composed of organometallic or coordination compounds, in which the access of substrates can be fine-tuned by means of appropriate ligand design, likewise strategies have not been successful in POM chemistry. Because of the chemical inertness of the M(VI)−O bonds (M = W or Mo), the covalent attachment of organic ligands to the metal−oxygen framework most often leads to product mixtures that display completely rearranged cluster cores with concomitant loss of their original catalytic activity.[5]

We recently described novel strategies to modify POMs while retaining their structural integrity and their intrinsic properties. One procedure employed rests on the exchange of the POM countercations with suitable surfactants, leading to so-called "surfactant-encapsulated clusters" (SECs).[6] Surfactant encapsulation is a versatile, highly economic procedure to alter the surface chemical properties of various POM compounds. The anionic cluster is nested within a shell of surfactants, thus leading to discrete, electrostatically neutral, hydrophobic core−shell particles, the structures and properties of which we have studied in great detail.[7] An alternative strategy is based on the exchange of the POM countercations with cationic macromolecules, leading to a novel type of POM/polyelectrolyte hybrid material.[8]

Here, we report on the structure and properties of $(C_{52}H_{60}NO_{12})_{12}[(Mn(H_2O))_3(SbW_9O_{33})_2]$, **3**, which is composed of a sandwich-type transition metal-substituted heteropolytungstate, **2a**, that is encapsulated within a shell of novel, dendritically branching amphiphiles, **1**. Compound **2a** was chosen because of its excellent performance in the homogeneous catalytic epoxidation of dienes.[9]

A central challenge in the characterization of complex soft materials lacking crystalline order is to establish quantitative structure−property relationships at a sufficiently accurate level. Therefore, we apply a combination of small angle neutron scattering and molecular dynamics simulations to reveal structural details of **3** at the nanoscopic scale.

Results and Discussion

In the following, we will describe first the preparation and characterization of SEC **3**, then the isostructural POM **2b** and its crystal structure (Figure 1), the coordinates of which are used in the following MD simulations, and finally, the characterization of **3** by SANS.

Characterization of SEC 3. The dendron-encapsulated cluster **3** was prepared according to previously published procedures.[7] The heteropolytungstate **2a** was dissolved in water, then the aqueous solution was treated with a trichloromethane solution containing dendron **1·Br** (Scheme 1). This resulted in spontaneous and complete transfer of **3** into the organic phase, which is easily seen by the color change of the two phases. Spectroscopic investigations (UV−vis and IR) showed the presence of both components in the self-assembled SEC. Although the characteristic UV−vis absorption band of **2a** (λ_{max} = 387 nm) remains unchanged upon encapsulation, some of its characteristic IR-bands are slightly shifted due to encapsulation. The UV−vis absorption bands of dendron **1** can be found at 283 and 243 nm, whereas its characteristic IR-frequencies occur at 3091, 3003, 2938, and 2839 cm^{-1} and in the fingerprint region. These measurements confirm that **3** is composed of both the POM **2a** and dendron **1**. They also demonstrate that the cluster anion remains intact and does not decompose upon encapsulation. The hydrophobic nature of **3** is demonstrated by virtue of its solubility: the SEC easily dissolves in organic solvents, such as $CHCl_3$, toluene, or THF, but is completely insoluble in water.

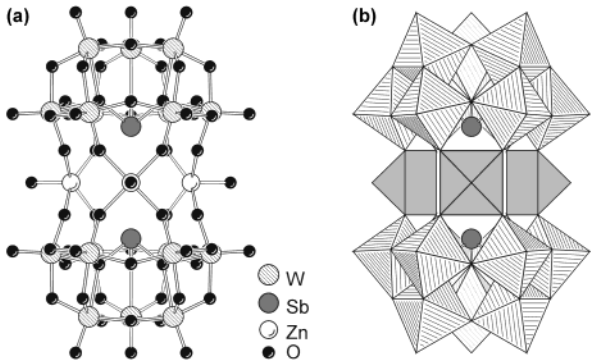

Figure 1. (a) Ball-and-stick and (b) polyhedral representation of the heteropolytungstate **2b** in the crystal structure of $Na_6K_6[(Zn(H_2O))_3(SbW_9O_{33})_2]\cdot 23H_2O$. (Counterions and water molecules are omitted for clarity.)

Scheme 1

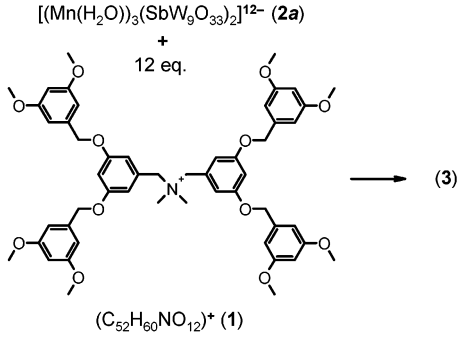

Elemental analysis of **3** indicated a complete exchange of alkali metal counterions. The POM anion is encapsulated in a shell of ∼12 dendrons, therefore yielding a molar mass of ∼15778 g/mol for the supramolecular entity **3**.[10]

The hydrodynamic radius of **3** was determined by analytical ultracentrifugation (AUC). From sedimentation velocity experiments, the sedimentation coefficient was calculated, which is $s = 6.34 \pm 2.9$ s. The diameter of **3**, as calculated from the

(5) Gouzerh, P.; Proust, A. *Chem. Rev.* **1998**, *98*, 77.
(6) Kurth, D. G.; Lehmann, P.; Volkmer, D.; Cölfen, H.; Müller, A.; Du Chesne, A. *Chem. Eur. J.* **2000**, *6*, 385.
(7) (a) Volkmer, D.; Du Chesne, A.; Kurth, D. G.; Schnablegger, H.; Lehmann, P.; Koop, M. J.; Müller, A. *J. Am. Chem. Soc.* **2000**, *122*, 1995. (b) Kurth, D. G.; Lehmann, P.; Volkmer, D.; Müller, A.; Schwahn, D. *J. Chem. Soc., Dalton Trans.* **2000**, 3989.
(8) (a) Caruso, F.; Kurth, D. G.; Volkmer, D.; Koop, M. J.; Müller, A. *Langmuir* **1998**, *14*, 3462. (b) Kurth, D. G.; Volkmer, D.; Ruttorf, M.; Richter, B.; Müller, A. *Chem. Mater.* **2000**, *12*, 2829.
(9) Bösing, M.; Nöh, A.; Loose, I.; Krebs, B. *J. Am. Chem. Soc.* **1998**, *120*, 7252.

(10) The molar mass presented here corresponds to the idealized stoichiometric ratio of 12:1 (dendron:POM). We are currently unable to quantify the exact (minor) amount of "defect" SECs corresponding to a substoichiometric ratio (11:1 or less). The ^{1}H NMR spectrum of the dendron-encapsulated cluster $(C_{52}H_{60}NO_{12})_{12}[(Zn(H_2O))_3(SbW_9O_{33})_2]$ displays broad signals that are significantly shifted against the (sharp) signals in the spectrum of free dendron (**1·Br**). As a result of the fact that signals of free **1·**Br are missing in the ^{1}H NMR spectrum of this SEC, we suggest a purity of at least 95%. Photometric measurements at λ_{max} = 387 nm, furthermore, prove that the (highly colorized) POM **2a** is completely transferred from the aqueous solution into the organic phase. We have, however, not yet been able to establish the appropriate mass spectroscopic techniques that would have shown a mass peak corresponding to nonfragmented SECs.

sedimentation coefficient, is $D = 2.7 \pm 0.5$ nm. The approximate dimensions of **2a** are $1.5 \times 1.1 \times 1.1$ nm, whereas the length of a single dendron **1** amounts to 1.3 nm, assuming a fully extended conformation. The diameter of SEC **3,** therefore, might be as large as 3.8 nm. The actual diameter, however, is considerably smaller, owing to the propensity of the dendron shell to adapt a dense packing. Since we could not observe decomposition or aggregation products by AUC, the experimentally determined hydrodynamic radius corresponds to single (monodisperse) SECs. In summary, we conclude that SEC **3** consists of a single POM cluster residing within a shell of 12 dendrons.

Crystal Structure of 2b. The open-shell electronic structure of the three μ-oxo-bridged high-spin Mn(II) centers gives rise to severe obstacles in calculating the electronic ground-state properties of **2a**. Since the primary goal here is to derive atomic partial charges being used for MD simulations, we restricted DFT quantum mechanics calculations on the Zn-substituted derivative **2b**, assuming (a) that the Zn-containing POM is isostructural with **2a** and (b) that the ground-state electron density distributions of **2a** and **2b**, respectively, are (almost) identical. To support this hypothesis, single crystals of **2b** were prepared, and the single-crystal X-ray structure of this novel POM compound was solved.

A ball-and-stick as well as a polyhedral representation of the Zn-substituted heteropolytungstate $[(Zn(H_2O))_3(SbW_9O_{33})_2]^{12-}$ (**2b**), derived from X-ray structure analysis, is shown in Figure 1. It was found that compound **2b** is isostructural with the Mn-containing heteropolytungstate (**2a**) reported earlier.[9] Compound **2b** contains two identical α-B-$[SbW_9O_{33}]^{9-}$ fragments (≡{Sb-W_9}) of the α-Keggin structure, consisting of three corner-sharing W_3O_{13} groups, and is closely related to similar sandwich-type POMs containing trivacant Keggin subunits.[11] The preparation procedure employed the lacunary {SbW_9} fragment as precursor, from which the sandwich-type heteropolytungstate **2b** can be generated at pH 7.5. The X-ray structure analysis of **2b** (for details, see Table 1) revealed a POM composed of two {SbW_9} subunits connected to each other by three zinc atoms in a belt. The zinc centers are coordinated by four oxygen atoms with an average $Zn-O_{W-Zn}$ bond length of 2.03 Å and one water molecule (Zn−O(W1) bond length, 2.01 Å) to complete a square-pyramidal coordination sphere. Positioned in the center of each {SbW_9} subunit, the Sb^{III} heteroatom shows a distorted ψ-tetrahedral coordination with a $Sb-O_{W3-Sb}$ bond length of 1.98 Å. Further selected bond lengths and angles are presented in Table 2.

Molecular Dynamics Simulations. MD simulations were performed in order to complement structural investigations on dendron-encapsulated clusters by means of SANS and to get further insights into the dynamic structure of the dendron shell. Since the supramolecular ensemble consists of some 1600 atoms, MD simulations at the ab initio level of theory are currently not applicable. Thus, we followed a molecular mechanics approach, using a modified Amber 94 force field[12] to define the intra- and intermolecular atomic interaction potentials.

Table 1. Crystal Structure Data of $Na_6K_6[(Zn(H_2O))_3(SbW_9O_{33})_2]\cdot 23H_2O$

	Na_6K_6[**2b**]·$23H_2O$
formula	$H_{52}Na_6K_6O_{92}Zn_3Sb_2W_{18}$
formula weight (M), g mol^{-1}	5645.84
crystal size, mm^3	$0.24 \times 0.4 \times 0.32$
crystal color/habit	colorless needles
crystal system	hexagonal
space group	$P6_3/mmc$ (no. 194)
a, Å	15.265(2)
c, Å	24.461(5)
V, Å^3	4936.3(14)
Z	2
ρ_{calc}, g cm^{-3}	3.763
μ, mm^{-1}	22.511
F(000)	4880
T, K	213(2)
2θ range	$9° < 2\theta < 52°$
reflections collected	36 960
independent reflections	1832 [R(int) = 0.1538]
GOF on F^2	1.227
R ($>2\sigma$ (I))	$R_1{}^a = 0.0488$ $wR_2 = 0.1278$
R (all data)	$R_1{}^a = 0.0512$ $wR_2 = 0.1294$
$(\Delta/\rho)_{max}$, e$^-$/Å^3	3.06
$(\Delta/\rho)_{max}$, e$^-$/Å^3	−4.71

[a] $R_1 = \Sigma||F_o| - |F_c||/\Sigma|F_o|$. [b] $wR_2 = |\Sigma w(F_0^2 - F_c^2)^2/\Sigma(F_0^4)]^{1/2}$. $w_1 = 1/[\sigma^2(F_o^2) + (0.0620P)^2 + 160.86P]$.

Table 2. Experimental and Calculated Bond Lengths (Å) and Angles (deg) of **2b** in Na_6K_6[**2b**]·$23\ H_2O$

	exptl	calc
W(1)−O(1), W(2)−O(5)	1.72(1)	1.79−1.80
W(1)−O(2)	1.92(1)	1.97
W(1)−O(3)	1.89(1)	1.92−1.93
W(1)−O(4)	2.40(1)	2.40
W(2)−O(3)	2.03(1)	2.08
W(2)−O(6), W(2)−O(7)	1.93(1)−1.96(1)	1.97−1.99
W(2)−O(4)	2.27(1)	2.32
W(2)−O(8)	1.79(1)	1.84
Sb(1)−O(4)	1.98(1)	2.05
Zn(1)−O(8)	2.03(1)	2.01−2.03
Zn(1)−O(W1)	2.01(1)	2.38
$O-W-O_{cis}$	73(1)−105(1)	73−105
$O-W-O_{trans}$	159(1)−170(1)	159−168
O−Sb−O	91(1)	90
$O-Zn-O_{cis}$	85(1)−103(1)	86−92
$O-Zn-O_{trans}$	154(1)	166

To model nonbonding electrostatic interactions between the cationic dendrons **1** and the negatively charged surface of **2a**, DFT calculations were performed, and different computational schemes were employed to derive partial atomic charges from the resulting electron density distribution. The primary criterion for the selected basis sets was to reproduce the experimental geometry of the $[(Zn(H_2O))_3(SbW_9O_{33})_2]^{12-}$ anion **2b**. The geometry of the isolated anion **2b** was optimized starting from a C_{3h}-symmetrical model structure. The symmetry elements are sustained during optimization. The theoretically calculated structure matches well with the experimental structure as derived from single-crystal X-ray structure analysis (Table 2). The most evident geometrical deviation concerned the Zn−O(W1) bond length (calculated, 2.38; found, 2.01 Å); the values of all other bond lengths and angles and the overall dimensions (intra-cluster distances) of the anion differed less than 5%, mostly around 2%. Mulliken as well as Löwdin atomic point charges for **2a**

(11) (a) Bösing, M.; Loose, I.; Pohlmann, H.; Krebs, B. *Chem. Eur. J.* **1997**, *3*, 1232. (b) Mialane, P.; Marrot, J.; Rivière, E.; Nebout, J.; Hervé, G. *Inorg. Chem.* **2001**, *40*, 44. (c) Loose, I.; Droste, E.; Bösing, M.; Pohlmann, H.; Dickman, M. H.; Rosu, C.; Pope, M. T.; Krebs, B. *Inorg. Chem.* **1999**, *38*, 2688.

(12) Cornell, W. D.; Cieplak, P.; Bayly, C. I.; Gould, I. R.; Merz, K. M., Jr.; Ferguson, D. M.; Spellmeyer, D. C.; Fox, T.; Caldwell, J. W.; Kollmann, P. A. *J. Am. Chem. Soc.* **1995**, *117*, 5179.

Table 3. Calculated Partial Charges for the **2b** Anion

atom	Mulliken partial charges	Löwdin partial charges
Zn(1)	0.928	0.783
O(W1)	−0.566	−0.568
O(8)	−0.592	−0.310 to −0.315
Sb(1)	1.172	0.967
O(4)	−0.775	−0.385
W(1/2)	1.383−1.435	0.250−0.361
O(1/5)	−0.591 to −0.621	−0.344 to −0.374
O(2/3/4)	−0.607 to −0.683	−0.304 to −0.372

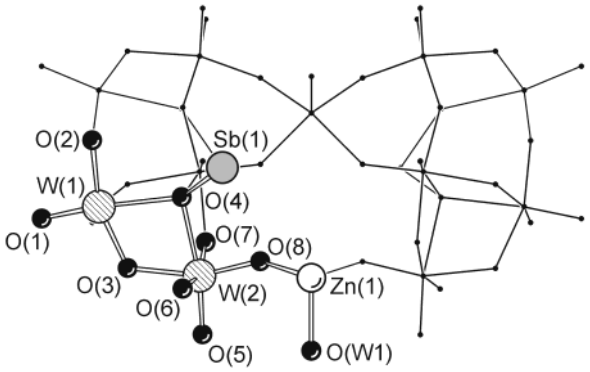

Figure 2. Numbering scheme of atoms in the asymmetric unit of the crystal structure of Na_6K_6[**2b**]·$23H_2O$ (orthographic projection).

were obtained from MO population analysis of POM **2b** and are listed in Table 3.

For MD simulations of SEC **3**, the trajectory of dendrons **1** at the surface of **2a** was calculated.

Figure 3 depicts a snapshot from a 100-ps MD simulation run at $T = 300$ K showing the typical supramolecular arrangement of dendrons pointing with their charged headgroups toward the cluster surface. Within the time limit of the MD simulation, no dissociative processes occurred, which would lead to an incompletely encapsulated cluster anion. To gain further insights into the packing density of the dendron shell, surface models of the solvent-accessible surface (SAS) were calculated for probe radii ranging from 0.1 to 10.0 Å.[13] The final solvent−accessible surface area ($\sqrt{A_{SAS}}$) is plotted versus probe radius in Figure 4. The deviation from the straight line, representing the SAS of a perfectly smooth sphere, becomes readily apparent for small probe radii. Similar calculations have been reported on carboxylic acid terminated PAMAM dendrimers of generation numbers 1−4,[14] in which dendrimers of generation 3 (and 4, respectively) reveal a greater internal than external surface area. These data were interpreted with the appearance of internal voids and clefts, indicating a porous dendrimer structure that should be readily accessible to guest molecules of the appropriate size. Our results suggest a porous shell structure in the SEC comparable to those of high-generation PAMAM dendrimers. However, in the case of the SEC, the porosity occurs already with first generation dendrons![15] Cavities and channels were visualized with surface contour models of **3** (Figure 5). The average pore size of these computer-generated structure models would let us assume a rather dense dendron packing arrangement, which should exclude access of medium to large-size molecules to the cluster surface. The elemental analysis of **3**, on the other hand, shows that a certain number of water molecules (≈15) reside within the SEC structure. It is not yet clear, however, if these water molecules are distributed throughout the dendron shell or if they are located close to the cluster surface.

(13) Average SAS values were calculated from 10 different configurations of a 100-ps trajectory at 10-ps time steps.
(14) Newkome, J. R.; Moorefield, C. N.; Vögtle, F. *Dendritic Molecules*; VCH−Wiley: 1996; p 28.
(15) It should be noted here that the total number (= 48) of terminal 3,5-(dimethoxy)benzyloxy moieties in the self-assembled dendron-encapsulated cluster is comparable to a covalently assembled Fréchet-type dendrimer of generation 4−5 (= 32 or 64 terminal groups).

Table 4. Scattering Lengths[a] Used in SANS Investigations

element	b_c [10^{-13} cm]
H	−3.739
D	6.671
C	6.6460
N	9.36
O	5.803
Cl	9.577
Mn	−3.73
Sb	5.57
W	4.86

[a] *Neutron News* **1992**, *3*, 29.

Table 5. Results from SANS

parameter	result
$d\Sigma/d\Omega$	$(Q = 0)$ 0.016 cm^{-1}
R_g	(1.44 ± 0.003)nm
$d\Sigma/d\Omega_{inc}$	0.0295 cm^{-1}
N	6.2×10^{17} cm^{-3}
Φ_{SANS}	1.74%
$\Phi_{nominal}$	2.25%

Small Angle Neutron Scattering of 3. To validate the proposed structure model of **3**, SANS investigations were carried out. This method was particularly well suited to investigate such a question, because the scattering contrast originates from the deuterated solvent in which the SEC is dissolved. The scattering pattern of **3** dissolved in a highly diluted $CDCl_3$ solution is depicted in Figure 6. Most of the scattering originates from single SECs. The enhanced scattering observed at small Q-values, however, indicates aggregation of a small fraction of clusters.

The scattering function shown in Figure 6 (solid line) was calculated by using the atomic coordinates as obtained from the MD simulations and tabulated values (see Table 4) of the atomic scattering lengths. Snapshots at 10 different evolution times between 0 and 100 ps were used for the calculations, and the resulting scattering functions were averaged thereafter. The parameters obtained from scattering were collected in Table 5. The size of the particles was derived from the radius of gyration $R_g = 1.44$ nm (eq 3) which, assuming a massive spherical particle, would yield a particle diameter of $D = 3.7$ nm according to the relationship $D = 2\sqrt{5/3}R_g$.[16]

The SANS particle diameter is in good agreement with the corresponding values of AUC measurements ($D = 2.67 \pm 0.54$ nm), or MD simulations (D ≈ 3.4 nm), respectively.

Summary and Outlook

In conclusion, we have presented a detailed picture of a novel surfactant-encapsulated polyoxometalate cluster, namely the dendron-encapsulated heteropolytungstate $(C_{52}H_{60}NO_{12})_{12}[(Mn(H_2O))_3(SbW_9O_{33})_2]$, **3**. Spontaneous self-assembly of the heteropolytungstate and the dendritic surfactant produces **3** at

(16) Guinier, A. *X-ray Diffraction*; W. H. Freeman and Company; San Francisco 1963; 329.

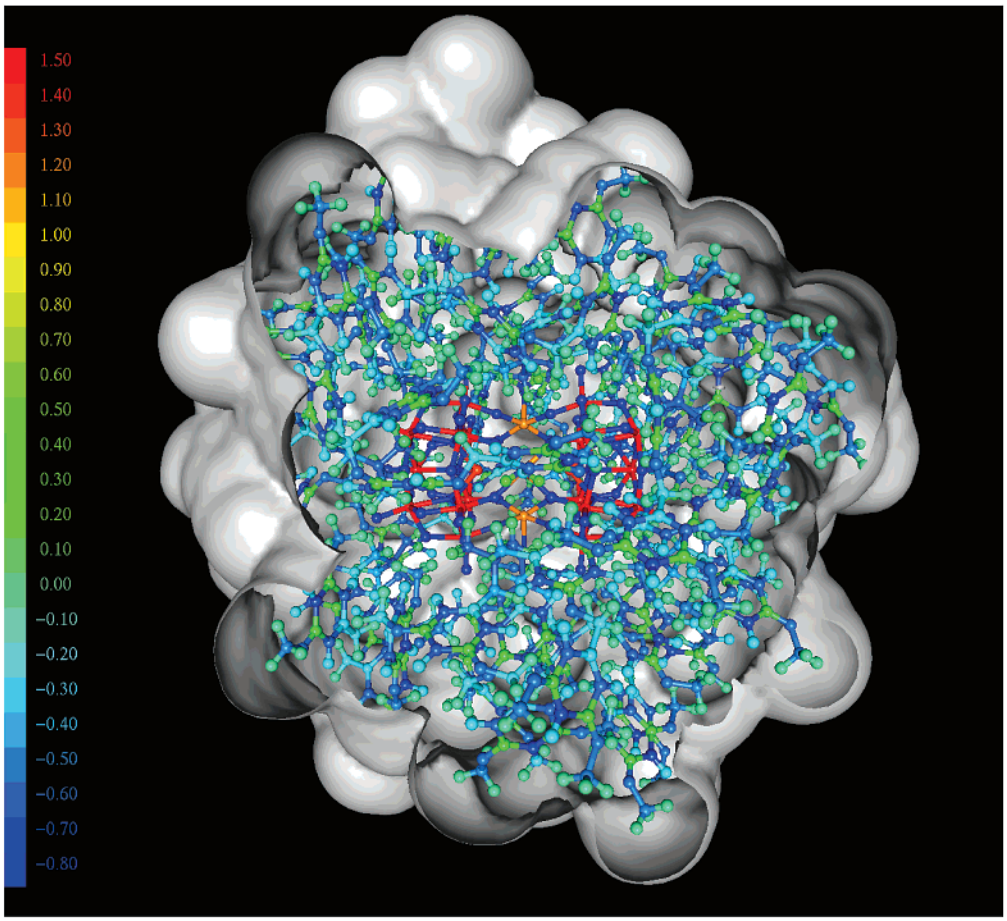

Figure 3. Snapshot taken from a molecular dynamics simulation of the dendron-encapsulated cluster **3**. Ball-and-stick model with color codes representing Mulliken atomic partial charges. The gray envelope displays the solvent accessible surface (SAS) calculated for a probe radius of 1.4 Å. (The foremost part of the SAS has been cut-away for clarity.)

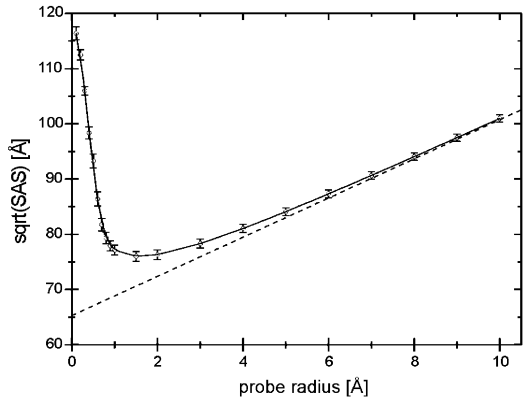

Figure 4. Plot of SAS values of **3**. Interpolated mean $(SAS)^{1/2}$ values for different probe radii ranging from 0.1 to 10 Å are depicted by the solid line. The dashed line represents the SAS function $(SAS)^{1/2} = 2\pi^{1/2}(r + r_p)$ for a hard sphere, where r is the radius of the sphere and r_p is the probe radius.

almost quantitative yield. This result shows that surfactant-encapsulation is a convenient and reliable approach to alter the surface properties of POMs and is widely applicable to different POM clusters and amphiphilic systems. To reveal details down to the nanoscopic level, we employed a combination of analytical (AUC, SANS, elemental analysis, UV−vis and IR spectroscopy) and computational methods (DFT calculations, MD simulations) in the structure analysis of SECs.

By encapsulating a catalytically active POM within a shell of cationic dendrons, we wished to combine the catalytic properties of POMs with the steric properties of the dendrons.[17] On the basis of size-exclusion principles, the dendron shell may thereby control access of substrates to the active site of the POM core and, thus, enhance the catalytic selectivity of the SEC. The propensity of high-generation dendrimers to form internal voids and cavities is a well-documented feature.[18] Following this concept, dendron-encapsulated POM clusters ("dendrizymes"[19]) bear a certain resemblance to natural metalloproteins.[20] In addition to many other studies, which are devoted to the isolation of active sites in dendrimer matrixes,[21] SECs appear particularly rewarding, considering the unsurpassed number of catalytically active POMs.[22] Future investigations will focus on the catalytic

(17) Catalytically active POM/dendrimer hybrid materials have been reported recently which consist of an organic, dendritically branched core and POM clusters covalently attached to the dendrimer periphery. Zeng, H.; Newkome, G. R.; Hill, C. L. *Angew. Chem., Int. Ed.* **2000**, *39*, 1771.
(18) Baars, M. W. P. L.; Meijer, E. W. *Top. Curr. Chem.* **2000**, *210*, 131.
(19) Brunner et al. have coined the term "dendrizymes" for metal complexes consisting of a dendritically branched (optically active) ligand and a strongly binding chelate core. (a) Brunner, H.; Altman, S. *Chem. Ber.* **1994**, *127*, 2285. (b) Brunner, H. *J. Organomet. Chem.* **1995**, *500*, 39.
(20) The apparent link between natural enzymes and catalytically active dendrimers has been pointed out by several authors. Selected reviews referring to this concept include (a) Fréchet, J. M. J. *Science* **1994**, *263*, 1710. (b) Smith, D. K.; Diederich, F. *Chem. Eur. J.* **1998**, *4*, 1353. (c) Cardona, C. M.; Mendoza, S.; Kaifer, A. E. *Chem. Soc. Rev.* **2000**, *29*, 37. (d) Gorman, C. B.; Smith, J. C. *Acc. Chem. Res.* **2001**, *34*, 60. (e) Twyman, L. J.; King, A. S. H.; Martin, I. K. *Chem. Soc. Rev.* **2002**, *31*, 69.
(21) Hecht, S.; Fréchet, J. M. J. *Angew. Chem., Int. Ed.* **2001**, *40*, 74.

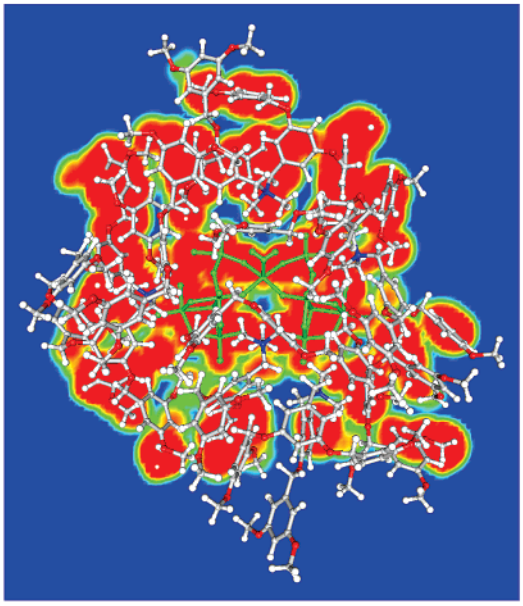

Figure 5. Ball-and-stick model of **3** displaying a SAS contour-plot projected onto a cut plane running through the center of the SEC. (Cluster **2a** appears green in color). Color-coded SAS contour levels correspond to surface probes with augmenting radii. (SAS probe radii ranging from 0.0 (red) to 1.4 Å (turquoise)). Blue regions that appear between the regions occupied by the dendron shell indicate internal cavities and clefts.

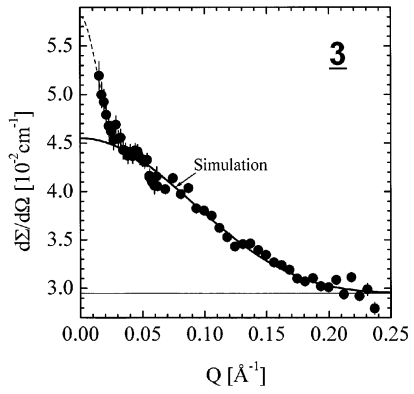

Figure 6. SANS results and theoretical curve from MD simulations of **3**.

performance of these novel dendrizymes, for which we are currently preparing a series of differently sized amphiphilic dendrons.

Our results show that MD simulations are becoming an indispensable tool to refine dynamic structure models of supramolecular systems, such as **3**, down to atomic resolution.

It should be pointed out that the computationally generated structure models inherently bear the danger of misleading interpretations. One critical point of the current MD simulations concerns the use of DFT-derived Mulliken partial charges in order to model electrostatic interactions. Although more powerful partition schemes have recently been developed to represent the electrostatic properties of small organic molecules,[23] these methods still remain to be extended to include compounds containing transition metal ions. Neglecting an atomistic representation of the solvent represents another simplification of the current structure model, which has been forced by the expense of a (certainly more realistic) solvent box model including some further 10 000 solvent molecules.[24] As a result of the lack of reliable experimental methods to adjust force field parameters of complex self-assembling structures, such as **3**, we decided to restrict our computational efforts to the present stage. However, at this level of analysis, our approach is readily available to the bench chemist to develop and test prototypes of artificial dendrizymes and related systems. The results of such types of analysis may also become important in understanding phenomena that occur on short-length scales, such as ion and electron transport or structural relaxation processes in soft materials.

Experimental Section

Preparative Procedures. Analytical TLC was performed on commercial Macherey-Nagel plates POLYGRAM ALOX N/UV_{254}. Columns were packed with aluminum oxide (activated, neutral, 0.05−0.20 mm). NMR spectra were recorded on a Bruker DRX 500 with the solvent signal as standard. Mass spectra were obtained on an Esquire 3000 with electrospray ionization.

IR spectra of $Na_6K_6[(Zn(H_2O))_3(SbW_9O_{33})_2]\cdot 23H_2O$ (Na_6K_6[**2a**]$\cdot 23H_2O$) were performed on a Perkin-Elmer 683 spectrometer in a range 4000−400 cm^{-1}.

Synthesis of Bis-{3,5-bis[3,5-(dimethoxy)benzyloxy]benzyl}-dimethylammonium bromide (1·Br). 3,5-Bis[3,5-(dimethoxy)benzyloxy]benzyl bromide[25] (2.00 g, 3.98 mmol) was dissolved in dry THF (50 mL). To this solution was added sodium carbonate (106 mg, 1.00 mmol) and dimethylamine (500 μL, 1.00 mmol, 2 M solution in dry THF). After stirring for 48 h at 20°C under argon, the insoluble compounds were separated by filtration, and the solvent was removed under vacuum. Upon column chromatography (MPLC, ALOX acetonitrile → acetonitrile/methanol 10:1), a colorless oil was obtained in 94% yield (910 mg; 937 μmol). ^{1}H NMR ($CDCl_3$): δ 6.74 (d, 4, J = 1.9), 6.68 (t, 2, J = 1.9), 6.55 (d, 8, J = 2.2), 6.33 (t, 4, J = 2.2), 5.00 (s, 8), 4.75 (s, 4), 3.75 (s, 24), 2.90 (s, 6); ^{13}C NMR ($CDCl_3$): δ 161.0, 159.9, 138.0, 129.0, 112.1, 105.3, 104.2, 99.9, 70.0, 68.0, 55.3, 48.7; MS (ES): m/z = 890 ([M − Br]$^+$). Anal. Calcd for $C_{52}H_{60}BrNO_{12}$ (970.94): C, 64.33; H, 6.23; N, 1.44. Found: C, 64.54; H, 6.23; N, 1.35.

$Na_{11}(NH_4)[(Mn(H_2O))_3(SbW_9O_{33})_2]\cdot 45H_2O$ ($Na_{11}(NH_4)$[2a]$\cdot 45H_2O$). The compound was synthesized as described previously.[9]

$Na_6K_6[(Zn(H_2O))_3(SbW_9O_{33})_2]\cdot 23H_2O$ (Na_6K_6[2b]$\cdot 23H_2O$). The precursor compound $Na_9[SbW_9O_{33}]\cdot 19.5H_2O$ was synthesized as described previously.[11a] $Na_9[SbW_9O_{33}]\cdot 19.5H_2O$ (6.0 g, 2.1 mmol) was dissolved in water (30 mL), and $ZnSO_4\cdot 7H_2O$ (1.04 g, 3.6 mmol) was added dropwise. The mixture was heated at 90 °C for 1 h. After the reaction solution was cooled to room temperature, KCl solution (12 mL, 1 M) was added. After 1 day, colorless crystals of $Na_6K_6[(Zn(H_2O))_3(SbW_9O_{33})_2]\cdot 23H_2O$ (Na_6K_6[**2b**]$\cdot 23H_2O$) were obtained. Yield: 4.4 g (0.78 mmol, 74%). Anal. Calcd. for $H_{52}Na_6K_6O_{92}Zn_3Sb_2W_{18}$: Na, 2.44; K, 4.16; Zn, 3.47; Sb, 4.31; W, 58.3. Found: Na, 2.61; K, 4.08; Zn, 3.52; Sb, 4.25; W, 58.18. IR (KBr, cm^{-1}): 3412 (vs) (ν(O−H)); 1615 (s) (δ(H−O−H)); 1115 (s); 948 (vs) (ν(W−O_t)); 882 (vs) (ν(W−O_e)); 745 (vs) (ν(W−O_c)); 465 (s) (ν(Sb−O)) (t, terminal; e, edge-sharing, c, corner-sharing).

$(C_{52}H_{60}NO_{12})_{12}[(Mn(H_2O))_3(SbW_9O_{33})_2]\cdot 15\ H_2O$ (3). $Na_{11}(NH_4)$[**2a**]$\cdot 45H_2O$ (31.6 mg, $5.36\cdot 10^{-6}$ mol) was dissolved in water (20 mL).

(22) (a) Hill, C. L.; Prosser-McCartha, C. M. *Coord. Chem. Rev.* **199**5, *143*, 407. (b) A series of 34 recent papers in a volume devoted to polyoxoanions in catalysis: Hill, C. L. *J. Mol. Catal.* **1996**, *114*, 1−365. (c) Mizuno, N.; Misono, M. *J. Mol. Catal.* **1994**, *86*, 319. (d) Okuhara, T.; Mizuno, N.; Misono, M. *Adv. Catal.* **1996**, *41*, 113. (e) Kozhevnikov, I. V. *Catal. Rev.-Sci. Eng.* **1995**, *37*, 311.

(23) Li, J.; Zhu, T.; Cramer, C. J.; Truhlar, D. G. *J. Phys. Chem. A* **1998**, *102*, 1820.

(24) Box models of such dimensions would require massive parallel computation on a (very) huge computer cluster employing hand-optimized program codes, which is clearly beyond the scope of the current investigations.

(25) Stewart, G. M.; Fox, M. A. *J. Am. Chem. Soc.* **1996**, *118*, 4354.

Twelve equiv of **1·Br** (6.43×10^{-5} mol = 62.5 mg) dissolved in trichloromethane (20 mL) were added, and the encapsulated cluster was transferred into the organic phase by gentle shaking of the biphasic solution. The organic phase was separated, evaporated, and dried for 3 days at 3 mbar (20 °C). Anal. Calcd. for $(C_{52}H_{60}NO_{12})_{12}[(Mn(H_2O))_3(SbW_9O_{33})_2]\cdot 15H_2O$: C, 47.05; H, 4.59; N, 1.00; O, 22.72. Found: C, 47.45; H, 4.79; N, 1.06; O, 23.13. The molar weight of the SEC was calculated according to the results of the elemental analysis to be 15 778 g/mol. Spectral data of SEC: UV−vis ($CHCl_3$); λ [nm]: 387, 283, 243. IR (KBr, cm^{-1}): 3442, 3091, 3003, 2959, 2938, 2839, 1600, 1460, 1431, 1376, 1347, 1323, 1300, 1205, 1156, 1055, 1019, 943, 869, 836, 775, 752, 713, 683, 514, 464, 438. The density of the SEC was determined with a DMA 5000 density meter (solvent $CHCl_3$) to be $\rho = 1.82$ g/cm^3.

Analytical Ultracentrifugation. Analytical ultracentrifugation was carried out with a Beckman Optima XL-I (Beckman Instruments, Palo Alto, USA) analytical ultracentrifuge. The centrifuge was equipped with an integrated scanning UV−vis absorption and Rayleigh interference optical system. Sedimentation velocity experiments were performed in toluene at a rotational speed of 60 000 rpm. The sedimentation coefficient was determined to be $s = 6.34 \pm 2.9$ s. The calculated diameter of the SEC is $d = 2.67 \pm 0.54$ nm.

From the movement of the sedimentation boundary, the sedimentation coefficient, s, was determined according to $\ln(r_b/r_m) = s\omega^2 t$, where r_b and r_m are the radial positions of the boundary and the meniscus, respectively, and ω is the radial velocity. A plot of $\ln(r_b)$ versus time gave a straight line of slope $s\omega^2$. The diffusion coefficient, D, is determined from the spreading of the sedimentation boundary. A plot of time, t, versus $[c_p/(dc/dr)]^2$ gave a straight line of slope $D/4\pi$. Here, c_p is the concentration in the plateau region and dc/dr is the concentration gradient at the boundary. The hydrodynamic particle diameter, R, was determined according to $d^2 = 18\eta s/(\rho_p - \rho_s)$, were η is the solvent viscosity and ρ_p and ρ_s are the densities of the particles and solvent, respectively. The molecular weight was determined from the Swedberg equation $M = sRT/D(1 - \bar{\nu}_p)$, where $\bar{\nu}$ is the experimentally determined partial specific volume, and ρ, the solvent density. The values of s and D were determined at different concentrations and extrapolated to zero concentration.[26]

Crystal Structure Determination. Diffraction experiments were performed on a STOE IPDS imaging plate system with Mo−Kα radiation ($\lambda = 0.71073$ Å) and with corrections for absorption (using DECAY/ABSCOR). The structures were solved by direct methods using SHELXS 97 and refined with SHELXL 97 (on F^2) by full-matrix least squares. All metal atoms were refined anisotropically; the oxygen atoms were refined isotropically. As usual in polyoxometalate chemistry, we found little disorder in the range of counterions and water molecules. Details of the crystal data collection, processing and structure analysis and refinement are summarized in Table 1. Further information, such as positional and thermal parameters, can be obtained from the cif-files presented in the Supporting Information.

DFT Calculations. DFT investigations on the polyoxometalate cluster (**2b**) and the amphiphilic dendrons (**1**) were performed using the TURBOMOLE package[27] employing the Becke88 exchange and the VWN/Perdew86 and correlation functionals and split valence basis sets incorporating polarization functions (SV(P)).[28] Relativistic effective core potentials (ECPs) were applied for Sb,[29] and W.[30] This chosen set was found to accurately model the cluster anion's geometry and the relevant bonding characteristics. In contrast, preliminary model investigations on smaller polyoxotungstate fragments (WO_4^{2-}) showed that extended basis sets (e.g., a triple-ζ valence TZV(P) set, while operating the aforementioned functionals) tend to overestimate the ionic W−O bonding character, yielding unreasonably high Mulliken and Löwdin point charges. On the other hand, replacing the Perdew86 correlation functional by more accurate but computationally more expensive functionals, such as the Lee−Yang−Parr (LYP) correlation functional, did not result in significant Mulliken and Löwdin point charge differences.[31]

Molecular Dynamics Simulations. MD simulations were performed with the HyperChem program suite.[32]

Molecular models of dendron **1** were readily obtained from Amber94 force field calculations. With respect to the highly flexible nature of the hydrophobic benzyl ether branches, the conformational space of **1** was scanned on the basis of the Metropolis search algorithm.[33] The conformational analysis yielded some 100 unique conformers, the energetically most favorable of which was subsequently used in a single-point DFT calculation, followed by population analysis.

Atomic coordinates and partial charges of **2a** were obtained from a DFT geometry optimization of a C_{3h}-symmetric model structure, on the basis of the crystallographic atomic positions of **2b**. A customized Amber94 force field was used to model atomic interaction potentials. The atomic positions of **2a** were fixed during simulation runs. An energetically equilibrated starting configuration of **3** was obtained by performing several high-temperature MD simulation runs (1200 K, 5−10 ps) that were interrupted by short cooling cycles (0 K, 1−2 ps). The final MD simulation included a heating period (10 ps), allowing the molecular ensemble to reach a final temperature of 300 K starting from 0 K, followed by a 100 ps MD simulation run at constant (total) energy. During simulation, the coordinate shifts of dendrons **1** were recorded at 1-fs intervals.

Solvent Accessible Surface (SAS). SAS calculations were performed with the program MSMS V2.53.[34] SAS values were computed on the basis of atomic coordinates of **3** that were extracted from a 100-ps trajectory at constant (10-ps) time steps ($T = 300$ K). Molecules were represented as a set of overlapping spheres, each having the van der Waals radius of its constituent atom. The SAS of a molecule is the trajectory of the center of a spherical probe of radius r_p (which represents an imaginary solvent molecule) rolling over the van der Waals surface of the molecule.[35]

Small-Angle Neutron Scattering (SANS). SANS experiments were performed at the KWS1 diffractometer of the research center in Jülich.[36] The concentration of the sample was 41 mg/mL, which corresponds to a volume fraction 0.0225. The measurements were performed with a

(26) Ralston, G. *Introduction to Analytical Ultracentrifugation*; Beckman Instruments: California, 1993.
(27) (a) Treutler, O.; Ahlrichs, R. *J. Chem. Phys.* **1995**, *102*, 346. (b) Eichhorn, K.; Treutler, O.; Öhm, H.; Häser, M.; Ahlrichs, R. *Theor. Chem. Acc.* **1997**, *97*, 119.
(28) (a) Becke, A. D. *Phys. Rev. A* **1998**, *38*, 3098. (b) Perdew, J. P. *Phys. Rev. B* **1986**, *33*, 8822.
(29) Bergner, A.; Dolg, M.; Küchle, W.; Stoll, H.; Preuss, H. *Mol. Phys.* **1993**, *80*, 1431.
(30) Andrae, D.; Häussermann, U.; Dolg, M.; Stoll, H.; Preuss, H. *Theor. Chim. Acta* **1990**, *77*, 123.
(31) For recent investigations on the effect of different methods, basis sets, and functionals on the partial charges of a hypothetical $WO_2(OH)_2$ molecule, see: Judd, D. A.; Nettles, J. H.; Nevins, N.; Snyder, J. H.; Liotta, D. C.; Tang, J.; Ermolieff, J.; Schinazi, R. F.; Hill, C. L. *J. Am. Chem. Soc.* **2001**, *123*, 886. The results in this paper (see Table 1) also support our initial finding that Hartree−Fock-type calculations overestimate the ionic bond character of polymetalate species.
(32) *Hyperchem Release 6.01*; HyperCube Inc.: Gainesville, FL, 2000.
(33) Metropolis, N.; Rosenbluth, A. W.; Rosenbluth, M. N.; Teller, A. H.; Teller, E. *J. Chem. Phys.* **1953**, *21*, 1087.
(34) Sanner, M. F.; Spehner, J.-C.; Olson, A. J. *Biopolymers* **1996**, *38*, 305.
(35) Tabulated van der Waals radii were taken from the website at www.webelements.com. Values used in SAS calculations are as follows: C, 1.70; H, 1.20; N, 1.55; O, 1.52 Å. For the other elements, tabulated ionic radii were employed because of the lack of substantiate van der Waals radii: Mn(II), high-spin, octahedral, 0.97 Å; Sb(III), 0.90 Å; W(VI), octahedral, 0.74 Å. The use of ionic radii is, strictly speaking, incorrect in terms of the mathematical definition of the SAS; in practice, however, the affected atoms are hidden in the POM framework and, thus, do not contribute to the SAS. The most critical value is the (uncertain) van der Waals radius of oxygen atoms belonging to the POM that was chosen here to equal the well-established value for organic compounds. As a result of the fact that the coordinates of the POM are fixed during MD simulation runs, internal cavities originate from different packing arrangements of the dendron shell, which consists of purely organic ligands. The (inadequate) representation of the POM surface topology adds a constant factor to the calculated SAS values, and the error thus introduced is negligible.
(36) A description of the SANS instrument is given in www.neutronscattering.de.

neutron wavelength of 0.7 nm, and the data were evaluated with a standard procedure subtracting background and scattering from the solvent. The data are given in absolute units as obtained from calibration with a secondary standard. This allows the determination of the particle-number density and the volume fraction from the scattering at $Q = 0$ in eq 4. The total coherent scattering lengths of the molecule and of the solvent molecules filling the same volume is given, respectively, as $\sum_{j=1}^{N} b_i = 2.867 \times 10^{-10}$ cm and $N\bar{b}_s = 4.475 \times 10^{-10}$ cm (Table 4). The molar volume was evaluated from the molar weight $M = 15520$ g/mol, and the corresponding density $d = 1.82$ g/cm^3, the molar weight, and the density of the $CDCl_3$ were $M_S = 120.39$ g/mol and $d_S = 1.5004$ g/cm^3, respectively. From $d\Sigma/d\Omega(0) = 0.016$ cm^{-1}, the number density of $n = 6.2 \times 10^{17}$ cm^{-3} and the volume fraction of 0.0174 was calculated, which is approximately 77% of the nominal one.

According to the classical scattering theory of J. J. Thomson and P. Debye,[37] the scattered intensity from molecular clusters consisting of N atoms and having a particle-number density of n clusters/unit volume is described by the macroscopic cross section

$$\frac{d\Sigma}{d\Omega}(\vec{Q}) = n\left|\sum_{j=1}^{N}(b_j - \bar{b}_S)\exp(i\vec{Q}\vec{r}_j)\right|^2 \quad (1)$$

as a function of the momentum transfer $Q = |\vec{Q}| = (4\pi/\lambda)\sin(\Theta/2)$ (λ, neutron wavelength; Θ, scattering angle). The b_j is the coherent scattering length of the jth atom positioned at $\vec{r}_j$, and $\bar{b}_S$ is the mean atomic scattering length of the solvent (Table 4). Equation 1 can be modified for the case of randomly oriented clusters.

$$\frac{d\Sigma}{d\Omega}(Q) = n\left(\sum_{j=1}^{N}(b_j - \bar{b}_S)\frac{\sin(Qr_j)}{Qr_j}\right)^2 \quad (2)$$

The scattering of dendron-encapsulated clusters can be described by the Guinier approximation according to

$$\frac{d\Sigma}{d\Omega}(Q) \cong \frac{d\Sigma}{d\Omega}(0)\exp[-R_g^2Q^2/3] \quad (3)$$

because their size is on the order of 4 nm, and the experimental Q range is between 0.2 and 2.4 nm^{-1}. R_g is the radius of gyration. The scattering at $Q = 0$ in eq 3 is

$$\frac{d\Sigma}{d\Omega}(0) = n\left|\sum_{j=1}^{N}(b_j - \bar{b}_S)\right|^2 = n\left(\sum_{j=1}^{N}b_j - N\bar{b}_S\right)^2 \quad (4)$$

It is determined by the difference of the total coherent scattering lengths of the molecules and of the solvent molecules filling the same volume. The scattering length of the solvent is thus calculated by using the N_S tabulated scattering-length values $b_{s,j}$ of the solvent molecule of molecular weight M_s and density d_s and by using the molecular weight M_c and the density d_c of the cluster.

$$\bar{b}_S = \frac{M_C d_S}{M_S d_C N}\sum_{j=1}^{N_S} b_{S,j} \quad (5)$$

Measuring the scattering intensity in absolute units delivers the particle-number density, n.

Equation 2 can be recast into a form that is computationally more convenient:

$$\frac{d\Sigma}{d\Omega}(Q) = n\sum_{i=1}^{N} p(r_i)\frac{\sin(Qr_i)}{Qr_i} \quad (6)$$

where $p(r_i)$ is the so-called pair-distance distribution function (PDDF) that represents the histogram of all existing distances $r = |\vec{r}_j - \vec{r}_k|$ between atoms j and k inside the molecule. It is weighted by the scattering lengths $b(\vec{r}_j)$ and $b(\vec{r}_k)$ at the positions $\vec{r}_j$ and $\vec{r}_k$, respectively.

$$p(r) = \left\langle\sum_{j=1}^{N}[b(\vec{r}_j) - \bar{b}_S][b(\vec{r}_j - \vec{r}) - \bar{b}_S]\right\rangle \quad (7)$$

The $\langle\ \rangle$ brackets indicate that the PDDF is the average over all orientations of $\vec{r}$. Because the number of atomic coordinates N is finite, the average is automatically obtained when all N^2 distances r are collected into a histogram consisting of dr wide bins. This sampling procedure is safe for our purposes as long as the bin width chosen is smaller than the resolution limit $dr < \pi/Q_{max}$ of the experiment. Q_{max} corresponds to the largest accessible scattering angle.

Acknowledgment. This project was funded by BMBF Grant no. 03N8618A/B. D.V. thanks the Deutsche Forschungsgemeinschaft for financial support. D.G.K. and P.L. thank the Max-Planck-Society for financial support. M.P. and B.K. gratefully acknowledge the support of the Fonds der Chemischen Industrie. The authors are thankful to Helmuth Möhwald for valuable discussions.

Supporting Information Available: The Crystallographic Information File (CIF) of $Na_6K_6[(Zn(H_2O))_3(SbWgO_{33})_2]\cdot 23H_2O$ (Na_6K_6[**2b**]$\cdot 23H_2O$). This material is available free of charge via the Internet at http://pubs.acs.org.

JA017613B

(37) Debye, P. *Ann. Phys.* **1915**, *46*, 809.